Pressure dependence of thermal transport properties

Anne M. Hofmeister*

Department of Earth and Planetary Sciences, Washington University, St. Louis, MO 63130

Edited by Ho-kwang Mao, Carnegie Institution of Washington, Washington, DC, and approved December 5, 2006 (received for review September 18, 2006)

Pressure (*P*) derivatives of thermal conductivity (*k*) and thermal diffusivity (*D*) are important to geophysics but are difficult to measure accurately because minerals, being hard and partially transparent, likely incur systematic errors through thermal losses at interfaces and spurious radiative transfer. To evaluate accuracy, repeat experiments for olivine [$(Mg_{0.9}Fe_{0.1})_2SiO_4$], quartz ($SiO_2$), and NaCl are examined in detail: these and other data on electrical insulators are compared with theory. At ambient conditions, *D* is underestimated in proportion to the number of contacts. As temperature (*T*) increases, spurious radiative transfer more than offsets contact loss. Compression of pore space and contact losses affect pressure derivatives, but these seem independent of *T*. Accurate (±2%) values of *D*(*T*) at 1 atm are obtained with the contact-free, laser-flash method. Other optical techniques do not pinpoint *D* but provide useful pressure derivatives. Published data on $\partial(\ln k)/\partial P$ at ambient conditions agree roughly with all available models, the simplest of which predicts $\partial(\ln k)/\partial P \sim \partial(\ln K_T)/\partial P$, where K_T is the bulk modulus. However, derivatives verified by multiple measurements are reproduced accurately only by the damped harmonic oscillator model. An improved database is needed to refine this model and to confidently extrapolate these difficult measurements to geophysically relevant conditions.

laser-flash analysis | thermal conductivity

Thermal transport properties play a crucial role in mantle convection, because this phenomenon results from competition between diffusion of heat, resistance to motion, and buoyancy forces. Thermal conductivity (k) and its relative thermal diffusivity,

$$D = \frac{k}{\rho C_p}, \qquad [1]$$

where ρ is density and C_P is heat capacity at constant pressure (P), are regulated by two different mechanisms. Transport of heat by phonons is termed lattice conductivity ($k_{\rm lat}$). For electrical insulators such as mantle minerals, photons also move heat. Radiative transfer inside Earth proceeds by diffusion among the grains and is calculated from spectroscopic measurements (e.g., ref. 1). In contrast, laboratory experiments involve direct (also called boundary-to-boundary) radiative transfer wherein photons emitted from heater warm the thermocouple with minimal participation of the sample, because most electrical insulators are transparent at certain frequencies (1–3). This effect is not easily separated from $k_{\rm lat}$. Recent advances made in measurement of D using the contact-free, laser-flash technique (4, 5) allow removal of unwanted direct radiative transfer effects from the raw data. Their approach was recently applied to Earth materials at T but not at P (6–9). Pressure studies of $k_{\rm lat}$ (or D) predominately involve conventional, contact methods (e.g., refs. 10–12), which potentially include simultaneous but opposing errors due to direct radiative transfer and contact resistance at interfaces (e.g., refs. 13 and 14).

This report uses laser-flash results and the existing database to decipher meaningful values of $\partial k_{\rm lat}/\partial P$. Single crystals are the focus for several reasons. (*i*) Grain boundary behavior, such as differential thermal expansion or compression of pore space, should be relatively unimportant inside the Earth because grain boundaries are well annealed at high T and P. (*ii*) Understanding heat transport in single crystals is a precursor to deciphering the more complicated behavior of agglomerates. (*iii*) Problems in measuring single crystals are likely present in studies of rocks but are more difficult to recognize. Comparisons are made at ambient conditions and at elevated P and T. The unfortunate conclusion is that contact methods yield problematic results for geophysically important silicates and oxides; most results are inaccurate and systematically underestimate $k_{\rm lat}$ or D at low T and overestimate values at high T. However, pressure derivatives are fairly consistent for multiple measurements and independent of temperature. Well constrained derivatives unaffected by compaction of pore space and deformation of the sample are reproduced accurately by the damped harmonic oscillator model.

Models of Vibrational Heat Transport

Debye's (15) analogy of the scattering of phonons to collisions of molecules in a gas forms the basis of all models of heat transport in electrical insulators. Peierls (16) and Klemens (17) derived summations of the form

$$k_{\rm lat} = \frac{1}{3}\frac{\rho}{ZM}\sum_{j=1}^{3}\sum_{i=1}^{3NZ} c_{ij}u_{ij}^2\tau_i, \qquad [2]$$

where M is the molar formula weight, Z is the number of formula units in the primitive unit cell, u_{ij} is the group velocity ($= d\omega_i/ds_j$), s_j is the wave vector, $\omega = 2\pi\nu_i$ is the circular frequency of a given mode, ν_i is frequency, τ_i is the mean free lifetime, $i = 1$ to $3NZ$ sums the normal modes of a crystal with N atoms in the formula unit, $j = 1$ to 3 sums the three orthogonal directions, and c_{ij} is the Einstein heat capacity of each vibrational mode, which depends on ν_i and T.

Acoustic Models. Given the success of Debye's model for C_V, parameters for acoustic modes have generally been used to calculate $k_{\rm lat}$, and optic modes were considered to play a minor part (e.g., ref. 18). One shortcoming is the need to estimate lifetimes (19, 20). Generally, τ_i is assumed to go as $1/T$ above the Debye temperature (θ, which is 500 K for mantle minerals), which reproduces Euken's (21) empirical law (16):

$$k_{\rm lat} = {\rm B}/T \text{ for } T > \theta. \qquad [3]$$

The factor B has been related to thermodynamic quantities. Julian (22) derived

$$k_{\rm lat} = \frac{24}{20}\frac{4^{1/3}}{\gamma_{th}^2}\left(\frac{k_{\rm B}\theta}{h}\right)^3\frac{ZMa}{T} \quad \text{for } T > \theta, \qquad [4]$$

where $\gamma_{\rm th} = \alpha V K_T/C_V$ is the thermal Grüneisen parameter, α is thermal expansivity, V is molar volume, K_T is the bulk modulus $= -V/(\partial V/\partial P)$, $k_{\rm B}$ is Boltzmann's constant, h is Plank's constant, and a^3 is the volume of the unit cell. Roufosse and Klemens (20) obtained the same form as Eq. **4**, but 1/7 as large.

Author contributions: A.M.H. performed research, analyzed data, and wrote the paper.

The author declares no conflict of interest.

Abbreviations: FWHM, full width at half-maximum; LFA, laser-flash analysis; LO, longitudinal optic; TO, transverse optic.

*E-mail: hofmeist@wustl.edu.

Based on Debye's heat capacity model, $\theta \propto \nu$ in Eq. **4**, giving

$$\frac{\partial(\ln(k_{\rm lat}))}{\partial P} = \frac{1}{K_T}\left(3\gamma_{\rm th} + 2q_{\rm th} - \frac{1}{3}\right) \approx \frac{6}{K_T} \quad \text{for } T > \theta, \qquad [5]$$

where the second Grüneisen parameter $q_{\rm th} = \partial\ln\gamma_{\rm th}/\partial\ln V$ (e.g., refs. 23 and 24). However, Debye's model severely restricts values of Grüneisen parameter due to assuming linear dispersion, i.e.,

$$u \sim \nu\alpha \sim \nu V^{1/3} \qquad [6]$$

for a cubic lattice across the Brillouin zone. For comparison, the definition of group velocity, using $s = 2\pi/a$ for the cubic lattice, gives

$$u_i \sim \gamma_i \nu_i V^{1/3}. \qquad [7]$$

Debye's model requires that mode Grüneisen parameters are constant and near unity, and thus $q_{\rm th} = 0$ is required for Eq. **5**.

Dimensional Analysis. Dugdale and MacDonald (25) also assumed that $\tau \sim 1/T$, providing

$$k_{\rm lat} = \frac{C_v}{3\alpha}\frac{u}{\gamma_{\rm th}}\frac{a}{T} = \frac{VK_T}{3}\frac{u}{\gamma_{\rm th}^2}\frac{a}{T}. \qquad [8]$$

In accord with their derivation, $\langle u\rangle$ is approximated as $(VK_T)^{1/2}$, the bulk sound speed, giving

$$\frac{\partial(\ln(k_{\rm lat}))}{\partial P} = \frac{1}{K_T}\left(\frac{3}{2}\frac{\partial K_T}{\partial P} + 2q_{th} - \frac{11}{6}\right) \approx \frac{6}{K_T}. \qquad [9]$$

Roughly, $q_{\rm th} = 1 + \delta_T - \partial K_T/\partial P$, where $\delta_T = (1/\alpha K_T)(\partial K_T/\partial T)$. This approximation for $q_{\rm th}$ omits terms on the order of 0.1 and provides values of $q_{\rm th}$ from 0 to 2 (e.g., ref. 26).

Bulk Sound Model. The summation in Eq. **2** is simplified to

$$k_{\rm lat} = \frac{\rho}{3ZM} C_V \langle u\rangle^2 \tau. \qquad [10]$$

Assuming that $\langle u\rangle$ is the bulk sound velocity provides

$$\frac{\partial(\ln(k_{\rm lat}))}{\partial P} = \frac{1}{K_T}\frac{\partial K_T}{\partial P} + \frac{1}{C_v}\frac{\partial C_v}{\partial P} + \frac{1}{\tau}\frac{\partial \tau}{\partial P} \cong \frac{K'}{K_T} \approx \frac{4}{K_T}. \qquad [11]$$

The middle term should be ≈1/10th of the first ($K'/KT \sim$ 4%/GPa), from the identity

$$\partial C_P/\partial P = -T\partial^2 V/\partial T^2 = -TV(\alpha^2 + \partial\alpha/\partial T) \qquad [12]$$

and available data (27). Pressure studies (11, 28) corroborate this inference for minerals, providing $\partial\ln(C_P)/\partial P \sim 0.4\%$/GPa, which is <1/10th of $\partial\ln(k_{\rm lat})/\partial P = 5\%$/GPa. Given the uncertainties in measuring $k_{\rm lat}(P)$, the heat capacity term can be dropped. The pressure dependence of the lifetimes should be small; for optic modes, this property is closely related to population of vibrational states (7) that are governed by temperature, not pressure (discussed further below). The last term is also negative because compression should provide more frequent collisions and hence shorter lifetimes. Thus, Eq. **11** sets an upper limit for $\partial k_{\rm lat}/\partial P$.

Optic Model. Lifetimes of optic modes are obtained through the damped harmonic oscillator model of Lorentz (e.g., refs. 7 and 29–31). For any given mode,

$$\tau_i = \frac{1}{2\pi \rm FWHM_i}, \qquad [13]$$

where $\rm FWHM_i$ is the full width at half-maximum from individual peaks in the dielectric functions that are extracted from IR reflectivity data (e.g., ref. 32). FWHM of Raman peaks are obtained directly from the spectra, although instrumental line broadening must be accounted for.

From Eqs. **2** and **7**, assuming that the mode Grüneisen parameters, $\gamma_i = (K/\nu_i)(\partial\nu_i/\partial P)$, where K pertains to the volume of the vibrating unit (26, 33), are roughly equal, and that a_i^3 on average equals the volume, gives

$$\frac{\partial(\ln(k_{\rm lat}))}{\partial P} = \frac{1}{K_T}\left(m\gamma_{\rm ave} + \frac{1}{3} - 2q_{\rm ave}\right) - \frac{1}{\langle \rm FWHM\rangle}\frac{\partial\langle \rm FWHM\rangle}{\partial P} \approx \frac{4}{K_T}, \qquad [14]$$

where $m = 2$ for $\theta > \approx$250 K, $m = 3$ for $\theta \sim$ 400 K, and $m = 4$ for $\theta > \approx$550 K (refractory mantle minerals). Previous derivations of $\partial\ln k_{\rm lat}/\partial P$ (29, 31) are missing the term $-2q$ because Eq. **6** was used in error. However, because q in Eq. **14** averages q_i, this should be very close to 0 (e.g., ref. 26). Roughly, $\gamma_{\rm ave}$ equals $\gamma_{\rm th}$.

Constraining FWHM(P) from IR measurements is difficult because of nonhydrostaticity and changes in the longitudinal optic (LO)–transverse optic (TO) splitting. Raman measurements above 100 K on ZnO, CuI, and $NaNO_3$ (34–36) give ∂(FWHM)/∂P near 0, whereas low-temperature slopes are larger: 1.3%/GPa for SiC; ≈5%/GPa for CuI, LaF_3, and Ge; and ≈12%/GPa for Si and the LO mode of ZnS that is affected by a resonance (37–40). The correlation of ∂(FWHM)/∂P with T could be due to the methanol-ethanol medium being stiffer at lower T. In this case, large slopes are probably not intrinsic, and ∂(FWHM)/∂P should be small compared with the compression term. Alternatively, oxides could have negligible changes in FWHM with P.

Comparison of Eqs. **5**, **11**, and **14** shows that acoustic models include large, positive dependencies of lifetimes on pressure: $\partial\ln\tau/\partial P = (\gamma_{\rm th} - 2/3)/K_T$. That lifetimes increase with pressure seemingly agrees with the correlation of $\tau \sim 1/T$ in acoustic models. However, most of the decrease in lifetime as T increases is attributable to increases in the number of phonons due to population of excited states. Population of states should not change with pressure, and the behavior of lifetime with P is not linked to changes with T.

Inference of Systematic Errors from Comparison of Various Experimental Methods

Dual-Contact Methods. Conventional measurements, wherein both the heat source and the thermocouples are in direct contact with the sample, are limited to ≈1,200 K because of limitations of the materials used, long measurement times, and radiative heat losses from the surface (41). Ångström's method or its variants dominate Earth science literature (e.g., ref. 12), wherein a sinusoidal source of heat at frequency ω is applied to one end of a rod-shaped sample, and the phase of the decaying sinusoidal temperature wave that passes into the sample is measured at a distance Z along the rod. The two-strip method (28) is probably the most accurate of the techniques used at moderate pressure for hard solids and single crystals. This and the transient hot wire technique provide k more accurately than D, ±6% and 30%, respectively (42). Osako *et al.* (11) used such a method.

Systematic errors arise from thermal contact resistance and differential thermal expansion (e.g., refs. 13 and 41). Surface roughness creates "gaps" through which phonons cannot propagate. This impediment is described as a thermal resistance. Because thermal resistances are additive (43), contact measurements underestimate $k_{\rm lat}$, in the absence of other problems.

Pressure derivatives of k obtained for hard solids may contain additional errors: deformation alters geometry, cracking reduces thermal contact, and resistivity is P-dependent (see refs. 10 and 44). In the older works, large uncertainties are associated with nonhy-

drostatic conditions and pressure calibration. We focus on recent work and omit results where cracking was reported.

Radiative transfer is recognized as a change in sign of $\partial \ln(k_{lat})/\partial T$ from negative to positive as T increases (e.g., refs. 2 and 3). This contribution is difficult to constrain for partially transparent minerals. It cannot be simply modeled, e.g., by using $k_{rad} \sim T^3$ (45) because this formula requires absorbance to be constant. Appropriate direct radiative transfer models that take into account experimental conditions such as sample length, ν and T dependence of sample absorption, and contact emissions have not yet been constructed.

Single-Contact Methods. In recent geophysical studies (46–48), heat was applied remotely, but the sample contacts thermocouples for determination of heat flow. The above problems associated with contacts and direct radiative transfer occur with this approach, which was demonstrated through application of a similar method to glasses (14). Data have not been collected at pressure.

Contact-Free, Laser-Flash Analysis (LFA). A thin plate (≈1 mm thick by ≈8 mm diameter) is held at temperature in the furnace while emissions from its upper surface are monitored remotely with an IR detector (41, 49). Additional heat to the lower surface is supplied remotely by an optical pulse from the IR laser. As heat from the pulse diffuses through the plate, the increase in emissions is recorded by the detector. Because emissions are directly related to temperature ($\approx T^4$), the detector response is known as a temperature–time curve. Surfaces of the sample are graphite-coated (≈1 μm thick) to absorb laser light, thereby shielding the detector, and to increase the intensity of the emissions (e.g., ref. 50). Equations used to analyze the data require that the pulse width be significantly shorter than the time it takes heat to cross the sample. Because the change in temperature across the sample associated with the pulse is small, ≈4 K, D is approximately constant during data acquisition, and the T dependence of D is determined solely by varying furnace temperature (41). By analogy to IR experiments (see ref. 51), use of thin plates minimizes the presence of unwanted LO modes; moreover, in this configuration, contact of the sample edges with furnace components is unimportant because emissions are collected from the center of the sample. The C coat, being thin and applied as a liquid, provides negligible contact resistance. The accuracy for the technique is considered to be 2%, determined through benchmarking against metals and graphite (52). These opaque and soft materials lack radiative transfer and have good thermal contact.

Direct radiative transfer is recognizable in the temperature–time curves as a virtually instantaneous rise in emissions after the laser pulse, whereas slow, vibrational transfer causes a gradual increase in emissions (e.g., see refs. 7 and 9). Thin metal coatings deposited before graphite are used to minimize radiative transfer (4). Mathematical modeling (5) separates these effects, as established through benchmarking (50).

Contact-Free, Optical Methods Used at Pressure. Picosecond transient grating spectroscopy has provided D at P (53). In brief, laser pulses crossing at an angle 2φ create an interference pattern with grid spacing $L = 0.5\lambda/\sin\varphi$. The signal decays as $\exp(-2t/\tau)$ and the diffusivity is obtained from the decay rate (τ) and a radiative component of thermal transfer (r) using $\tau^{-1} = 4\pi^2 D/L^2 + r$. Decay is measured by Bragg diffraction of a third laser pulse. Because measurements are at 298 K, r is negligible. If long-lived electronic states participate, then τ reflects processes in addition to thermal relaxation, and D is underestimated.

Pangilinan *et al.* (44) developed an all-optical technique involving decay of a thermal wave and applied this to NaCl at pressure. A thermal model is used to extract both k and D.

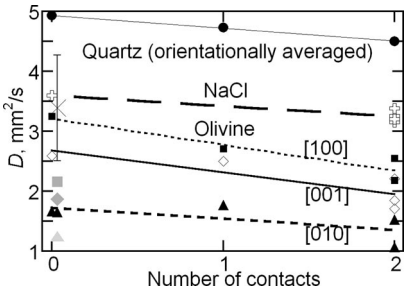

Fig. 1. Thermal diffusivity at room temperature as a function of the number of physical contacts with heaters and/or thermocouples. All lines are least squares linear fits to the data. Squares, diamonds, and triangles, three orientations as labeled of olivine, ~$Mg_{1.8}Fe_{0.2}SiO_4$ (3, 9, 48, 63, 64); gray symbols, picosecond transient grating spectroscopy measurements of olivine (53), which have problems other than contact (see text); circles, weighted average of the two orientations of quartz, SiO_2 (3, 47, †); +, NaCl (24, 54, 66, 67): LFA results of D = 3.6 mm²/s is the average of 10 measurements on a crystal purchased from IR Crystal Laboratories; ×, NaCl from Pangilinan *et al.* (44).

Existing Database on Vibrational Heat Transport in Electrically Insulating Solids

Evaluating the accuracy of pressure derivatives requires first examining measurements at ambient conditions. Temperature effects are considered as many studies elevate P and T simultaneously.

Effect of Contact on Measurements at Ambient Conditions. Only for a few minerals do multiple measurements of single crystals exist that use all of the above classes of methods (Fig. 1). Variations in chemical composition or disorder preclude comparing many minerals. For olivine, $Mg_{1.8}Fe_{0.2}SiO_4$, slight sample variations occur but are unimportant because San Carlos material was mainly studied, and laser flash analysis gave the same D values for different samples with similar compositions (9). Extrapolations from high temperature are excluded because D changes rapidly near 298 K.

Recent measurements of essentially pure, synthetic NaCl are included because this has been the focus of many heat transport studies at pressure. The average of the four contact studies shown in Fig. 1 is 3.25 mm²/s, which closely compares to the average of earlier data (see ref. 54). For NaCl, D is reduced from laser-flash results by 4% per contact. For quartz (SiO_2), which is also highly pure, D is reduced by 5% per contact. For olivine, orientationally averaged values are reduced by 13% per contact. "Dry" Mg-Fe-Mn garnets behave similarly (7), but this comparison includes uncertainties due to compositional differences.

Significantly less scatter is observed in the correlations of D with the number of contacts if average values rather than individual orientations are compared (Fig. 1). This difference exists because individual orientations are affected by polarization mixing. Using very tall cylinders in single-contact measurements (48) makes the olivine axis with the highest D yield values much lower than laser-flash results, whereas the axis with lowest D has higher values than laser-flash results, and D for the intermediate axis from both methods is similar. That long samples mix polarizations is supported by LFA data on one piece of olivine at various thicknesses. We found that at a height-to-diameter ratio, h/d, of 0.1, LFA provides intrinsic values of D, but that D is elevated by 20% in thick samples, i.e., when h/d = 0.2 (9).

Contact-free, picosecond transient grating spectroscopy (53) provides $D \sim 25\%$ low for olivine (Fig. 1). Values for garnet from picosecond transient grating spectroscopy seem low as well (7). Processes in addition to thermal relaxation apparently contribute to

†Branlund, J. M., Hofmeister, A. M., American Geophysical Union Fall Meeting, Dec. 13–17, 2004, San Francisco, CA, abstr. T41B-1208.

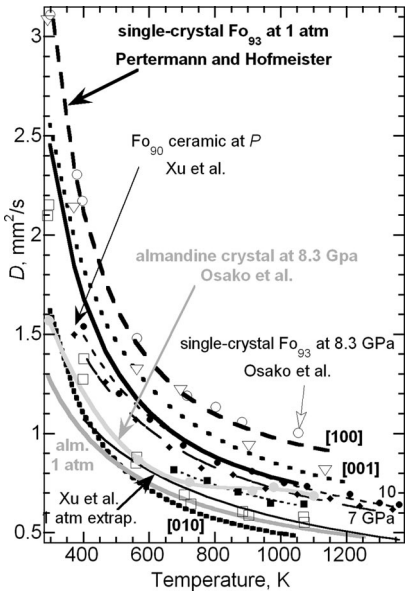

Fig. 2. Recent data on $D(T)$ for hard, dense materials at various pressures. Dark gray, single-crystal garnet ($Mg_{0.21}Fe_{0.74}Ca_{0.05}Al_2Si_3O_{12}$) from LFA at 1 atm (7); light gray and squares, single-crystal garnet ($Mg_{0.24}Fe_{0.74}Ca_{0.01}Al_2Si_3O_{12}$) at 8.3 GPa (11): the fit is a third-order polynomial in T; black symbols and lines, olivine, $Mg_{1.8}Fe_{0.2}SiO_4$; dots, aggregates at 10 GPa; filled diamonds, 7 GPa; filled squares, 4 GPa (12); light broken lines, fits to $D = a + b/T$; solid line, extrapolation of data of Xu *et al.* (12) to 1 atm; open circles, triangles, and squares, orientated single-crystal olivine at 8.3 GPa (11); heavy broken lines, oriented single-crystal olivine from LFA at 1 atm (9); heavy solid line, orientational average of LFA. High-P contact measurements underestimate D. In addition, single crystals are effected by radiative transfer at high T.

the rate of decay of the laser pulse. Absolute values of D from optical method of Pangilinan *et al.* (44) are also uncertain (Fig. 2); see their discussion for details.

Conventional measurements for olivine rocks and ceramics provide $D \sim 40\%$ below LFA values (55), whereas contact results for single-crystal data are low by $\approx 25\%$ (Fig. 1). Although preferred orientation explains some of this additional discrepancy for the rocks, this does not apply to ceramics, suggesting that contact resistance existing between grains in polycrystalline samples reduces D from intrinsic values.

Temperature Dependence at Pressure: Is Separation of Variables Warranted? Recent contact studies of olivine at P and T examined ceramics (12) and single crystals (11). At all T, $\partial D/\partial T$ of the ceramics at the various pressures investigated nearly parallels the trend in LFA data (Fig. 2), consistent with fine-grained ceramics suppressing radiative transfer. Below 700 K for [010] or 900 K for [100] and [001], D from contact measurements of single-crystals parallels LFA results, but at higher T, the contact measurements of D level off or slightly increase with T (Fig. 2). This behavior is consistent with spurious radiative transfer increasing as T increases. Comparison of single-crystal garnets (7, 11) in Fig. 2 supports this conclusion. Parallelism with LFA below 700 K indicates that the pressure response is separable from temperature effects at these low T and furthermore suggests that it is valid to separate variables in theoretical models.

Do Contact Measurements Provide Absolute Values of D Under Compression? Extrapolation of the data of Xu *et al.* (12) to 1 atm (1 atm = 101.3 kPa) provides D similar to LFA of the [010] axis with the lowest D value. Preferred orientation was not detected, and is not expected for their fine grain-size, so D of the ceramic at 1 atm should instead nearly equal the average of the three orientations. At 1,000 K, the average of the single-crystal measurements (9) is 0.77 mm^2/s, and contact measurements (12) are below this by 0.20 mm^2/s (33%). At 400 K, the average of the single-crystal measurements is 1.69 mm^2/s, and the ceramics are below this by 0.61 mm^2/s (36%). Room temperature was not accessed at pressure, and the slope is considerably steeper near 298 K than 400 K. The data are insufficiently accurate to constrain the room temperature value through fitting, i.e., fits to $D = B_0 + B_1/T$ (Fig. 2) or B/T^m (see ref. 12) have similar residuals. Based on a comparison of the measurements of olivine of Xu *et al.* (12) to LFA data, we suggest that their results underestimate D of wadsleyite and ringwoodite by $\approx 33\%$ for $T >$ 400 K and more near 298 K.

Measurements of $D(T)$ for single-crystal olivine at 8.3 GPa (11) nearly coincide with curves obtained by LFA at 1 atm (Fig. 2). On average, using the pressure dependence determined by Osaka *et al.* (11), their D values are low by ≈ 0.5 mm^2/s ($\approx 30\%$). That this discrepancy is smaller than that inferred in the measurements of Xu *et al.* (12) may be due to use of a different contact method or to additional thermal resistance between the grains of the ceramic. For garnet, D is only underestimated by 0.06 mm^2/s ($\approx 5\%$) compared with LFA results (7, 11). It seems that the amount of contact resistance depends on the specific experiment. This is not new: uncertainties of 20% have been associated with conventional methods (e.g., ref. 10). Apparently, compression does not remove this systematic error, and absolute values of D are not provided by contact methods at pressure.

Pressure Derivatives. One concern is the accuracy to which pressure was determined, which is difficult to gauge for older studies, and there may be systematic differences between studies that use external vs. internal calibrations. A few studies are dismissed: those in which the sample cracked, which creates thermal resistance, or was porous, for which compression works to reduce porosity (see footnotes of Table 1). Such problems artificially elevate the pressure derivative. Results for fused silica and quartz (56) are omitted from analysis because these have much higher derivatives than measurements by Kieffer *et al.* (57), wherein the samples cracked.

Pressure can improve thermal contact, and thus the derivative of k_{lat} will be incorrect if progressive compression alters the interface. Comparing data at two different elevated pressures should provide accurate derivatives, whereas comparing data at ambient and elevated pressure potentially overestimates $\partial D/\partial P$. Because k_{lat} linearly depends on pressure for all materials except $NaClO_3$ and S and pressure ranges of the various experiments overlap, pressure derivatives should be unaffected by the starting pressure or range of pressures in the experiments. (Only one study exists for $NaClO_3$ and S, so comparisons cannot be made for these cases.) The compilation in Table 1 provides evidence for compaction problems at very low P: values for $\partial \ln(k_{lat})/\partial P$ of olivine decrease rapidly as the maximum P in the experiment increases. This progression is clearly not intrinsic, because it is an order of magnitude larger than theoretical predictions. Problems at very low pressure are attributed to initial compression of the thermal contacts, pore space, grain rotation, or trace interstitial phases. Our inference is supported by similar pressure derivatives being obtained from an optical method (53), and by the three very-high-pressure studies (11, 12, 58), which did not involve comparison with 1-atm measurements (Table 1). Pressure derivatives from low-P studies of granular rocks are unlikely to represent intrinsic behavior for hard materials.

Pressure derivatives obtained from polycrystals of olivine and NaCl appear to give higher-pressure derivatives than single crystals of the same compositions (Table 1). This difference is not correlated with porosity because the samples were well compacted, and for the case of olivine, microscopic examination was conducted. Deformation and annealing of the softer salt crystals should have removed pore space.

Studies of NaCl give $k^{-1}\partial k/\partial P$ near 30%/GPa, including early work summarized by Ross *et al.* (10). The derivatives of MacPher-

Table 1. Pressure derivatives of thermal conductivity from contact methods

Sample	Form	P_{max}, GPa	$k^{-1}\partial k/\partial P$, %/GPa	Ref.
Mg_2SiO_4	Ceramic	0.5	16*†	68
$Mg_{1.8}Fe_{0.2}SiO_4$	Ceramic	0.2	12*†	69
	Dunite	1	9, 10, 12*†	70
	Crystal	4.8	≈4.8‡	53
	Dunite	5.6	6, 7*	58
	Crystal	5.6	5, 6*	58
	Crystal	8.3	3.2, 3.4, 3.8*	11
	Ceramic	9	5.5*†§	71
	Ceramic	10	4.4*	12
MgO	Ceramic	5	≈4.0*	72
	Crystal	1.2	5.0	28
	Crystal	5	2.0	59
NaCl	Crystal	5.6	18	59
	Crystal	5	17	58
	Crystal	4	31	73
	Polycrystal	4	32.7	24
	Polycrystal	2	31	54
	Polycrystal	2	30.7	66
	Polycrystal	1.8	36*	57
	Crystal	1.7	27*‡	44
SiO_2 glass	Slab	9	−3.7	74
	Slab	1	−4	75
	Slab	1.0	6†	56
Quartz ⊥c	Crystal	1.2	50†	56
Quartz, both	Crystal	1.2	29†	56
Coesite	2% porosity	4	3.9†	73
	Polycrystal	5.6	1.4–4.4	58
Stishovite	1% porosity	4	9†	73
$Py_{25}Al_{74}Gr_1$	Crystal	8.3	4.6	11
$Mg_{0.85}Fe_{0.15}O_3$	Crystal	5.6	7	76
$\sim NaAlSi_2O_6$	Unknown	3	4.6	11
Sulfur	Polycrystal	2	69	77
CaF_2	Crystal	1.0	11	23
$NaClO_3$	Polycrystal	2	32	78
LiF	Crystal	1	12	23
LiBr	Polycrystal	2	28.9	65
RbF	Polycrystal	2	34.4	65
CsI	Polycrystal	2	41	54
NaF	Polycrystal	4	14.9	24
NaBr	Polycrystal	4	60.2	24
NaI	Polycrystal	4	77.1	24
	Polycrystal	2	69	66

Earlier literature on $k^{-1}\partial k/\partial P$ of alkali halides are summarized by Ross *et al.* (10). Multiple values for $k^{-1}\partial k/\partial P$ indicate that several pieces or orientations were measured in the cited study. We omit contact data on MgO by Yukatake and Shimada (73) and on SiO_2 glass and quartz by Kieffer *et al.* (57) because their samples cracked, and on quartz by Beck *et al.* (58) because their sample partially converted to coesite. Thermodynamic and elastic parameters from literature compilations (27, 33, 60–62) or cited in the above references on k and D.

*Calculated from $k^{-1}\partial k/\partial P \sim 1/K_T + D^{-1}\partial D/\partial P$ (see text).

†Omitted from Fig. 4 because of compression of pores or problems with low P measurements.

‡Contact-free, optical method.

§Contains 5% enstatite, which has a higher pressure derivative.

son and Schloessin (59) and Beck *et al.* (58) from crystals seem low. The grain boundaries may have an effect because the optical study of Pangilinan *et al.* (44) gives 27%/GPa, which is lower than the average value that is skewed by data on polycrystals (Table 1). Deformation of this relatively soft material may account for the discrepancies. The variance in $k^{-1}\partial k/\partial P$ for NaCl, which has been measured more than any other substance, suggests that the accuracy of unconfirmed measurements is a concern.

Many measurements (lower part of Table 1, except CsI, which was measured twice by the same group) are uncorroborated, and their pressure derivatives must be considered uncertain in view of

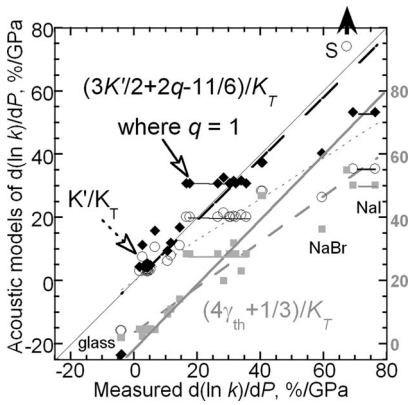

Fig. 3. Comparison of calculated to measured pressure derivatives of thermal conductivity. Diamonds and long dashed line, prediction using Dugdale and McDonald's model; circles and dotted line, comparison with K'/K_T; gray squares, comparison with optic model (left y axis). Sulfur, NaI, and NaBr data (labeled) strongly affect the slope. For sulfur, the model of Dugdale and McDonald (25) predicts 112%/GPa (as indicated by the arrow). Results for NaCl and NaI are each joined by lines.

the above comparisons. Again, some older studies were omitted as concerns exist regarding the accuracy of pressure calibrations. The soft materials are of great concern, because of the variation in $k^{-1}\partial k/\partial P$ among studies of NaCl and the fact that most soft materials were polycrystalline and measured only once. It may be that the only trustworthy pressure determinations of k_{lat} (or D) are of NaCl because of the shear number of studies, and of the single crystals and ceramics measured at very high pressure (MgO, olivine, garnet, fluorite, and pyroxene).

Comparison of Measured Pressure Derivatives of Thermal Conductivity with Models

Measured (Table 1) and calculated pressure derivatives are compared at 298 K in Fig. 3, ignoring the restriction of Eqs. **5** and **9** to high temperature. The fits shown are model as a function of measurements, which does not gauge predictive capabilities. Fit of the measurements as a function of the calculations (in units of %/GPa, with the intercept constrained to be zero and the negative derivatives for glass omitted) have some uncertainties because of the scatter in the data:

$$\partial \ln k_{lat}/\partial P \text{ (measured)} = 1.18\ \partial \ln k_{lat}/\partial P \ (R = 0.93, \text{ Eq. } \mathbf{14})$$

$$\partial \ln k_{lat}/\partial P \text{ (measured)} = 1.40\ \partial \ln k_{lat}/\partial P \ (R = 0.87, \text{ Eq. } \mathbf{11})$$

$$\partial \ln k_{lat}/\partial P \text{ (measured)} = 0.93\ \partial \ln k_{lat}/\partial P \ (R = 0.86, \text{ Eq. } \mathbf{9})$$

$$\partial \ln k_{lat}/\partial P \text{ (measured)} = 1.75\ \partial \ln k_{lat}/\partial P \ (R{=}0.93, \text{ Eq. } \mathbf{5}).$$

The fitting coefficients being greater than unity is consistent with omission of lifetimes depending on P. Fits to the acoustic model are not shown in Fig. 3 but are obviously poor from the above equation: this model can be dismissed on the basis of slope. The bulk sound model also has an overly large slope but reasonably fits hard solids, which are the most trustworthy measurements (those that have $0 < \partial \ln k_{lat}/\partial P < 20$%/GPa, except for NaCl, which is the long line of points in Fig. 3). Part of the mismatch may be due to using $K' = 5$, which is not well contained for most of the alkali halides. The dimensional analysis of Dugdale and McDonald (25) reasonably matches the measurements overall if $q = 1$ (Fig. 3), but this overestimates $\partial \ln k_{lat}/\partial P$, because of this model's assuming a large dependence of τ on P, which is not correct. The optic model has a low amount of scatter and closely reproduces the trustworthy measurements. For the optic model, we used $q = 0$, which is in line

with spectroscopic data on hard materials (most frequencies linearly depend on pressure).

Fig. 3 shows that the data on the alkali halides and sulfur, which are very soft substances, are scattered about all of the models. This observation supports the above contention that deformation is a likely problem in the contact measurements of these overall soft materials.

Conclusions

Methods involving contact, commonly used in geologic science, involve systematic errors. Major problems are the presence of unwanted direct radiative transfer and resistance at contact interfaces. The laser-flash technique avoids these problems, but one drawback is that the sample size required is too large for measurement of high-pressure synthetics. Improving the accuracy and precision in determining heat transport properties requires further implementation of this and other all-optical techniques to a greater variety of minerals and high-pressure structures.

Available data indicate that the P and T components of D (or of k_{lat}) can be modeled separately and recombined to provide data at mantle conditions. Acoustic models and dimensional analysis do not reproduce observed behavior of D. Pressure derivatives are readily predicted from the optic model (Eq. **14**), because thermal Grüneisen parameters and bulk moduli are well known. For hard minerals, $\partial \ln k_{lat}/\partial P$ is also well represented by K'/K_T (Eq. **11**). The uncertainty in K' for many materials reduces the accuracy of prediction; however, hard materials (mantle phases) cluster near a K' of 4 (the harmonic value) and are amenable to use of Eq. **11**.

This work was supported by National Science Foundation Grants EAR-0207198 and EAR-0440088.

1. Hofmeister AM (2005) *J Geodyn* 40:51–72.
2. Lee DW, Kingery WD (1960) *J Am Ceram Soc* 43:594–607.
3. Kanamori H, Fujii N, Mizutani H (1968) *J Geophys Res* 73:595–605.
4. Degiovanni A, Andre S, Maillet D (1994) in *Thermal Conductivity*, ed Tong TW (Technomic, Lancaster, PA), pp 623–633.
5. Mehling H, Hautzinger G, Nilsson O, Fricke J, Hofmann R, Hahn O (1998) *Int J Thermophys* 19:941–949.
6. Buettner R, Zimanowski B, Blumm J, Hagemann L (1998) *J Volcanol Geotherm Res* 80:293–302.
7. Hofmeister AM (2006) *Phys Chem Miner* 33:45–62.
8. Hofmeister AM, Pertermann M, Branlund J, Whittington AG (2006) *Geophys Res Lett*, 10.1029/2006GL026036.
9. Pertermann M, Hofmeister AM (2006) *Am Mineral* 91:1747–1760.
10. Ross RG, Andersson P, Sundqvist B, Bäckström G (1984) *Rep Prog Phys* 47:1347–1402.
11. Osako M, Ito E, Yoneda A (2004) *Phys Earth Planet Inter* 143–144:311–320.
12. Xu Y, Shankland TJ, Linhardt S, Rubie DC, Langenhorst F, Klasinski K (2004) *Phys Earth Planet Inter* 143–144:321–326.
13. Fried E (1969) in *Thermal Conductivity*, ed Tye RP (Academic, London), Vol 2, pp 253–275.
14. Lee HL, Hasselman DPH (1985) *J Am Ceram Soc* 68:C12–C13.
15. Debye P (1914) *Vortrage über die Kinetische Theorie der Materie und der Electrizität* (Teuber, Berlin).
16. Peierls RE (1929) *Ann Phys Leipzig* 3:1055–1101.
17. Klemens PG (1958) *Solid State Phys* 7:1–98.
18. Slack G (1979) *Solid State Phys* 34:1–73.
19. Ziman JM (1962) *Electrons and Phonons: The Theory of Transport Phenomena in Solids* (Clarendon, Oxford).
20. Roufosse MC, Klemens PG (1973) *Phys Rev B* 7:5379–5386.
21. Eucken A (1911) *Ann Phys Leipzig* 34:186–221.
22. Julian CL (1965) *Phys Rev A* 137:128–137.
23. Andersson S, Bäckström G (1987) *J Phys C Solid State Phys* 20:5951–5962.
24. Pierrus J, Sigalas I (1985) *J Phys C Solid State Phys* 19:1465–1470.
25. Dugdale JD, MacDonald DKC (1955) *Phys Rev* 98:1751–1752.
26. Hofmeister AM, Mao HK (2002) *Proc Nat Acad Sci USA* 99:559–564.
27. Fei Y (1995) in *Mineral Physics and Crystallography: A Handbook of Physical Constants*, ed Ahrens TJ (Am Geophys Union, Washington, DC), pp 29–44.
28. Andersson S, Bäckström G (1986) *Rev Sci Instrum* 57:1633–1639.
29. Hofmeister AM (1999) *Science* 283:1699–1706.
30. Hofmeister AM (2001) *Am Mineral* 86:1188–1208.
31. Hofmeister AM (2004) in *Infrared Spectroscopy in Geochemistry, Exploration Geochemistry, and Remote Sensing*, eds King P, Ramsey M, Swayze G (Mineral Assoc Can, Ottawa), pp 135–154.
32. Spitzer WG, Miller RC, Kleinman DA, Howarth LW (1962) *Phys Rev* 126:1710–1721.
33. Hofmeister AM, Mao HK (2003) *Geochim Cosmochim Acta* 66:1207–1227.
34. Serrano J, Manjon FJ, Romaro AH, Widulle F, Lauck R, Cardona M (2003) *Phys Rev Lett* 90:055510.
35. Serrano J, Cardona M, Ritter TM, Weinstein BA, Rubio A, Lin CT (2002) *Phys Rev B* 66:245202.
36. Jordan M, Schuch A, Righini R, Signorini JF, Jodl H-J (1994) *J Chem Phys* 101:3436–3443.
37. Debernardi A, Ulrich C, Syassen K, Cardona M (1999) *Phys Rev B* 59:6774–6783.
38. Liarokapis E, Anastassakis E, Kourouklis GA (1985) *Phys Rev B* 32:8346–8355.
39. Ulrich C, Anastassakis A, Syassen K, Debernardi A, Cardona M (1997) *Phys Rev Lett* 78:1283–1286.
40. Serrano J, Cantarero A, Cardona M, Garro N, Lauck R, Tallman RE, Ritter TM, Weinstein BA (2004) *Phys Rev B* 69:014301.
41. Parker JW, Jenkins JR, Butler PC, Abbott GI (1961) *J Appl Phys* 32:1679–1684.
42. Hammerschmidt U, Sabuga W (2000) *Int J Thermophys* 21:1255–1278.
43. Carslaw HS, Jaeger JC (1959) *Conduction of Heat in Solids* (Oxford Univ Press, New York), 2nd Ed.
44. Pangilinan GI, Ladouceur HD, Russell TP (2000) *Rev Sci Instrum* 71:3846–3852.
45. Clark SP, Jr (1957) *Trans Am Geophys Union* 38:931–938.
46. Schilling FR (1999) *Eur J Mineral* 11:1115–1124.
47. Höfer M, Schilling FR (2002) *Phys Chem Miner* 29:571–584.
48. Gibert B, Schilling FR, Gratz K, Tommasi A (2005) *Phys Earth Planet Inter* 151:129–141.
49. Bräuer H, Dusza L, Schulz B (1992) *Interceram* 41:489–492.
50. Blumm J, Henderson JB, Nilson O, Fricke J (1997) *High Temp High Pressures* 34:555–560.
51. Berreman RG (1963) *Phys Rev* 130:2193–2198.
52. Blumm J, Opfermann J (2002) *High Temp High Pressures* 34:515–521.
53. Chai M, Brown JM, Slutsky LJ (1996) *Phys Chem Miner* 23:470–475.
54. Håkasson B, Andersson P, Bäckström G (1988) *Rev Sci Instrum* 59:2269–2276.
55. Hofmeister AM, Pertermann M, Branlund JM, in *Treatise in Geophysics*, ed Schubert G (Elsevier, Amsterdam), in press.
56. Horai K, Sasaki J (1989) *Phys Earth Planet Inter* 55:292–305.
57. Kieffer S, Getting WIC, Kennedy GC (1976) *J Geophys Res* 81:3018–3024.
58. Beck AE, Darba DM, Schloessin HH (1978) *Phys Earth Planet Inter* 17:35–53.
59. MacPherson WR, Schloessin HH (1982) *Phys Earth Planet Inter* 29:58–68.
60. Sumino Y, Anderson OL (1984) in *CRC Handbook of the Physical Properties of Rocks*, ed Carmichael S (CRC, Boca Raton, FL), Vol 3, pp 139–280.
61. Knittle E (1995) in *Mineral Physics and Crystallography: A Handbook of Physical Constants*, ed Ahrens TJ (Am Geophys Union, Washington, DC), pp 98–142.
62. Anderson OL, Isaak DG (1995) in *Mineral Physics and Crystallography: A Handbook of Physical Constants*, ed Ahrens TJ (Am Geophys Union, Washington, DC), Vol 3, pp 64–96.
63. Kobayashi Y (1974) *J Phys Earth* 22:359–373.
64. Osako M (1997) *Bull Natl Sci Mus Tokyo Ser E* 20:1–7.
65. Håkasson B, Ross RG (1989) *J Phys Condens Matter* 1:3977–3985.
66. Håkasson B, Andersson P (1986) *J Phys Chem Solids* 47:355–362.
67. Brydsten U, Gerlich D, Bäckström G (1983) *J Phys C Solid State Phys* 16:143–146.
68. Fujisawa H, Fujii N, Mizutani H, Kanamori H, Akimoto S (1968) *J Geophys Res* 75:4727–4733.
69. Staudacher W (1973) *Z Geophys* 39:979–988.
70. Gibert B, Schilling FR, Tommasi A, Mainprice D (2003) *Geophys Res Lett*, 10.1029/2003GL018459.
71. Katsura T (1995) *Geophys J Int* 122:63–69.
72. Katsura T (1997) *Phys Earth Planet Inter* 101:73–77.
73. Yutatake H, Shimada M (1978) *Phys Earth Planet Inter* 17:193–200.
74. Katsura T (1993) *Phys Chem Miner* 20:201–208.
75. Andersson S, Dzhavadov L (1992) *J Phys Condens Matter* 4:6209–6216.
76. Schloessin HH, Dvorak Z (1972) *Geophys J R Astron Soc* 27:499–516.
77. Nilsson O, Sandberg O, Bäckström G (1982) *ETPC Proc* 8:159–165.
78. Franson Å, Ross RG (1983) *J Phys C Solid State Phys* 12:2861–2869.